Seventh Framework Programme FP7-SPACE-2010-1
Stimulating the development of downstream GMES services

Grant agreement for: Collaborative Project. Small- or medium scale focused research project
Project acronym: **SIDARUS**
Project title: **Sea Ice Downstream services for Arctic and Antarctic Users and Stakeholders**

Grant agreement no. 262922
Start date of project: 01.01.11
Duration: 36 months
Project coordinator: Nansen Environmental and Remote Sensing Center, Bergen, Norway

D6.2: Ice thickness retrieval from CryoSat-2

Due date of deliverable: 31.12.2012

Actual submission date: 20.01.2014

Organization name of lead contractor for this deliverable: UCAM

Project co-funded by the European Commission within the Seventh Framework Programme, Theme 6 SPACE		
Dissemination Level		
PU	Public	X
PP	Restricted to other programme participants (including the Commission)	
RE	Restricted to a group specified by the consortium (including the Commission)	
CO	Confidential, only for members of the consortium (including the Commission)	

ISSUE	DATE	CHANGE RECORDS	AUTHOR
0.1	31.12.2013	Version 0.1	P. Wadhams

SIDARUS CONSORTIUM

Participant no.	Participant organisation name	Short name	Country
1 (Coordinator)	Nansen Environmental and Remote Sensing Center	NERSC	NO
2	Alfred-Wegener-Institut für Polar-und Meeresforschung	AWI	DE
3	Collecte Localisation Satellites SA	CLS	FR
4	University of Bremen, Institute of Environmental Physics	UB	DE
5	The Chancellor, Masters and Scholars of the University of Cambridge	UCAM	UK
6	Norwegian Meteorological Institute, Norwegian Ice Service	Met.no	NO
7	Scientific foundation Nansen International Environmental and Remote Sensing Centre	NIERSC	RU
8	B.I. Stepanov Institute of Physics of the National Academy of Sciences of Belarus	IPNASB	BR

Table of Contents

SUMMARY

This report has analyzed the sensitiviy of ice thickness rerieval from CryoSat2, based on input data regarding snow and ice density, ice density, water density, as well as the error sources for the thickness retrievals. Different algorithms for retrieval of thickness from freeboard measurements have been analyzed. The results of the analysis is used in the validation of CryoSat retrieved ice thickness presntedin D6.4.

1 Introduction

Model simulations and observations confirm the decline of sea ice thickness (SIT) and hence sea ice draft (SID) in the Arctic. The aim of this study is to develop, validate and select algorithm for SIT retrieval from CryoSat2. The new developed A(FD2) algorithm for CryoSat2 is validated with collocated SID from ULS and SIT from laser altimeter (LA) on board Operational Ice Bridge (OIB) by comparison of SIT and SID derived from ULS and LA with collocated SID data. The CryoSat2 A(FD2) algorithm with minimum bias is selected. The accuracy of the FD algorithm is confirmed by comparison of SID and SIT derived from collocated moored and on Submarine ULS, LA and RA. ESA/CryoSat2, NSIDC, climate change, cryosphere and numerical prediction models will benefit the results of this document

2 Ice thickness retrieval from CryoSat2 and laser altimeter

The algorithms to retrieve sea ice thickness (SIT) and sea ice draft (SID) from radar and laser altimeters and corresponding uncertainties are discussed in the following section.

2.1 Sea Ice draft and SIT retrieval from radar and laser altimeters using the equation for hydrostatic equilibrium

Assuming hydrostatic equilibrium, the SIT, h_i, can be retrieved from the freeboard, h_{fi}, measured from CryoSat2 (Figure 2.1) by:

$$h_i=(h_s\rho_s+h_{fi}\rho_w)/(\rho_w-\rho_i), \quad (2.1)$$

where the snow depth (h_s) and density (ρ_s) from Warren climatology [Warren, 1999] (WC) as a function of latitude, longitude and month of the year in the Arctic have been used until now [Laxon et al, 2012].

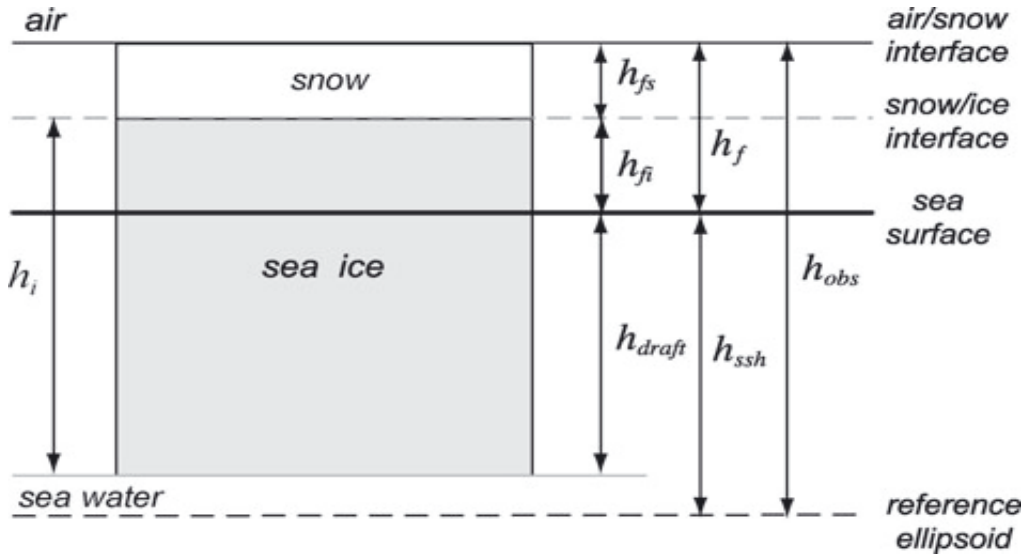

Figure 2.1: Computation of sea ice thickness from ice freeboard measured by radar and laser altimeter.

Assuming that the radar returns are from the snow–ice interface, which is valid for low temperature and dry snow, the SID, retrieved from RA is calculated as:

$$d_{ra}=h_i-h_{fi} = (h_s\rho_s+h_{fi}\rho_i)/(\rho_w-\rho_i), \quad (2.2)$$

where h_i is the SIT, calculated by Equation 2.1, and h_{fi} is the retrieved freeboard from radar altimeter. Water density, ρ_w, and ice density, ρ_i, depend on temperature, salinity and ice type, but to simplify the algorithm, constant values have been used from different authors, leading to incompatible results and errors in estimated SIT from RA [Connor et al, 2009, Laxon et al, 2012]. Seven algorithms for freeboard to SIT conversion have been compared, validated and the impact of sea ice density, snow depth density and water density has been examined [Djepa and Wadhams, 2013]. The validation (with ULS and OIB/laser altimeter) and sensitivity analyses demonstrated that the assumption of the half snow depth over first year ice (FYI) and fixed ice densities over FYI and MYI will lead to underestimation of the SIT.

The SIT, retrieved from the airborne laser altimeter (LA/ATM) on board Operational Ice Bridge (OIB), has been used for algorithm selection and validation. The SIT, retrieved from LA [Kurtz et al 2012] is snow depth, density, ice density and freeboard dependent as the SIT retrieved from RA and is calculated from the freeboard retrieved from the airborne laser scanner (h_f) at the air-snow interface by:

$$h_i = \rho_w h_f/(\rho_w-\rho_i)-(\rho_w-\rho_s)h_s/(\rho_w-\rho_i) \quad (2.3.)$$

where (h_s), is the snow depth, r_i , r_s , r_w are the ice, snow and water densities. The laser altimeter measures the freeboard on air snow interface, h_f, and the radar altimeter measure the freeboard on ice snow interface in the presence of dry snow and cold conditions (Figure 2.1).

2.2 Algorithms for sea ice thickness retrieval from CryoSat2

The CryoSat2 (A2) algorithm for freeboard to SIT conversion, used from Laxon et al (2013), to calculate the sea ice mass balance in the Arctic is based on equation for hydrostatic equilibrium (Equation 2.1), assuming fixed ice and water densities (ρ_{ify} = 916.7 kg m^{-3} for FY ice and ρ_{iMY} =882 kg m^{-3} for MYI, ρ_w=1030 kg/m^3), snow depth and density from WC and half of the snow depth from WC (h_{sfy}=0.5h_s (WC)) over FYI. In presence of FYI and MYI within altimeter averaged area, the ice density and snow depth are calculated by:

$$\rho_i = fr(FY)\ 916.7 + (1-fr(FY))882 (kg/m^3), \quad (2.4)$$

$$h_s = 0.5 fr(FY) * h_s\ (WC) + (1-fr(FY)) h_s\ (WC) \quad (2.5)$$

where h_s(WC) and the fraction, fr(FY), of FYI from the RA averaged area can be taken from OSI–SAF for limited period (since 2005). The SID, retrieved from the freeboard, applying CryoSat-2 algorithm is calculated and compared with collocated SID(ULS) (Figure 2.2.).

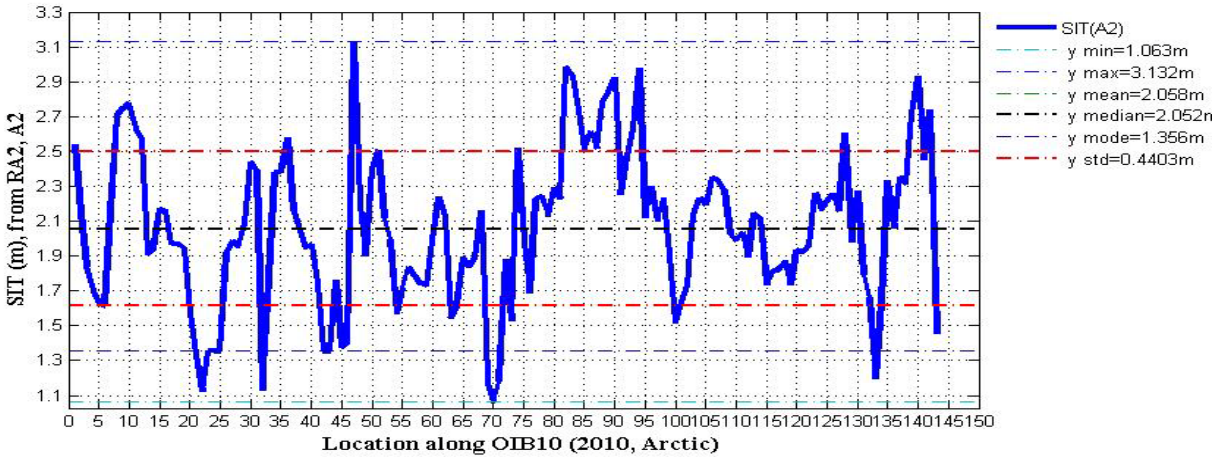

a)

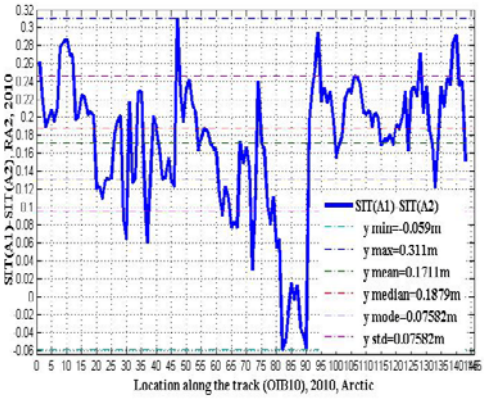

b)

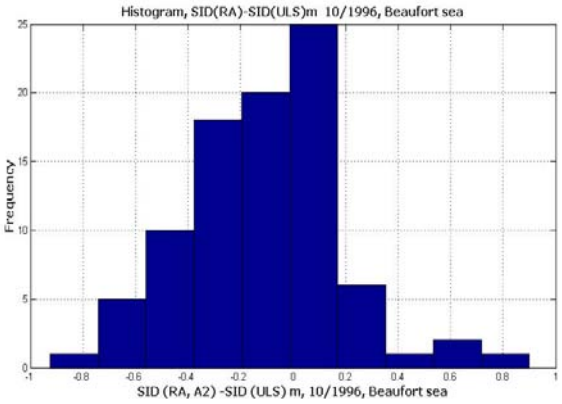

c) ε = -0.111m

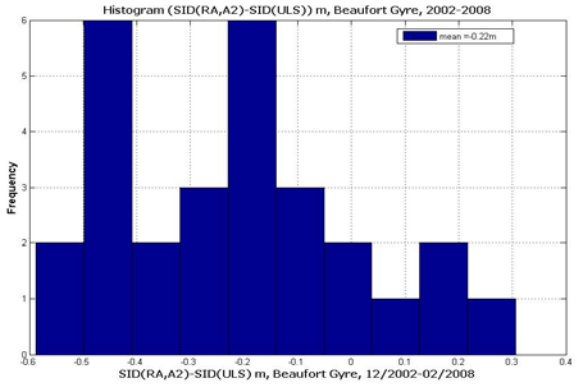

d) e = -0.265m

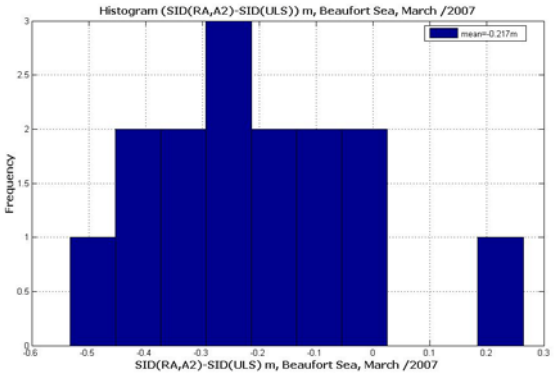

e) e = -0.26 m

Figure 2.2. SID, calculated by A2 (CryoSat2) algorithm. a) SIT (A2), 2010; b) SIT(A1)-SIT(A2), 2010; c) SID(A2)-SID(ULS), Beaufort Sea, 1996; d) SID(A2)-SID(ULS), Beaufort Gyre, 2002-2008; e) SID(A2)-SID(ULS), Beaufort Sea, 2007.

The comparison of SID(CryoSat2) with independent SID(ULS) in different locations within 7 years and comparison of SIT(A2) with SIT(A1) (Figure 2.2/c) demonstrated that the Cryosat2 algorithm always underestimates the SID and SIT.

The algorithm proposed by Hendricks, et al, (2013) is not applicable for SIT or SID retrieval from CryoSat-2 because there are fundamental errors in the equation provided and the assumptions, leading to unrealistic negative sea ice draft and SIT estimates, using F derived from RA.
Because the CryoSat algorithm underestimates the SIT and SID and the Hendricks et al (2013) algorithm gives negative values for retrieved SIT, new algorithms have been developed to retrieve SIT from CryoSat2.

Sensitivity study and uncertainty analyses have been applied to identify the impact of ice, snow and water density and snow depth on retrieved SIT from the freeboard measured from RA and to develop the new algorithms.

2.3 Sensitivity of retrieved SIT on input parameter variability

The assumptions of fixed ice density for FYI and MYI and half snow depth over FYI of CryoSat-2 algorithm have been tested applying sensitivity analyses. The equation (Equation 2.1.) for freeboard to SIT conversion is used for sensitivity analyses, with snow density and depth from WC, water density ri=1025kg/m3 and ice density (720- 950kg/m3). Assuming hydrostatic equilibrium, using ice density, 916.7+35.7kg/m3 (used in CryoSat-2 Algorithm), with snow depth 0.05m over FYI will produce SIT=1.096m with uncertainties +0.2717m for hfi=0.1m and the SIT uncertainty will increase, when snow depth, density and ice freeboard increase. If the area with MYI is misclassified as a FYI, use of a constant (wrong) FY ice density (916.7kg/m3) instead of MYI density (882kg/m3) will lead to SIT=4.4086+1.093m (for hfi=0.45m) instead of SIT=3.3388+0.4626m, overestimating SIT by 1.0698+0.63m for the same snow depth. SIT will be underestimated with 1.2m for hfi=0.2m if the snow depth is decreased 2 times (from hs(WC)=0.44m to hs=0.5hs(WC)) over FYI (CryoSat-2 algorithm).

SIT, calculated assuming ri =900kg/m3, rw=1030kg/m3, rs =300kg/m3, hfi=0.3m, hs=0.3m) will be underestimated by 0.35m (from 3.07m to 2.72m) if we assume half snow depth (hs=0.5(WC)) over FYI and the error will increase if hfi increase.

SIT calculated, applying CryoSat2 algorithm (ri =882kg/m3, rw=1030kg/m3, rs =300kg/m3, hfi=0.3m, hs=0.3m) will be underestimated by 0.42m (from 3.11m to 2.69m) if we assume half snow depth (hs=0.5(WC)=0.15m) over FYI and the error will increase if hfi and hs increase.

Snow density also impacts the accuracy of the retrieved SIT. SIT will be underestimated by 0.15m (from 3.12m to 2.97m) assuming ri =900kg/m3,

rw=1030kg/m3, hfi=0.3m, hs=0.3m, (A1 algorithm) if we use rs =260kg/m3 (Used from OIB2009) instead of rs =320kg/m3 (Used from OIB2010). For snow depth 30 cm and sea ice density in the range 720 to 950kg/m3, the uncertainty in the calculated SIT due to impact of ice density is up to 1.08m.

The uncertainties will differ for different snow depth and freeboard and this requires use of ice density calculated along the track as a function of freeboard and snow depth. The simulations confirmed the dependence of ice density and SIT on freeboard, snow depth and density, as well as the sensitivity of the retrieved SIT from RA on accuracy of the input information for ice and snow density, freeboard and snow depth.

The uncertainties of the retrieved SIT from CryoSat-2 will be discussed in the next section.

3 Factors impacting the accuracy of the retrieved SIT from CryoSat2

Considering sensitivity analyses and Equation 2.1., the main sources of errors of the SIT derived from the Cryosat-2 are : i) sea ice freeboard retrieval from CryoSat-2; ii) SIT retrieval from h_{fi} (Equation 2.1.) and absence of a-priori information for snow and ice type, density and snow depth;

3.1 Errors associated with the determination of sea ice freeboard

The elevation of the sea ice or lead is calculated by fitting a model to determine the first arrival time (τ) of the echo at the satellite position at point Z from the surface. This echo delay is converted to elevation by:

$$h_{obs} = z - c\tau/2 \qquad (3.1)$$

where c is the velocity of light and hobs is the elevation of an ice floe with respect to the reference ellipsoid.

The error in the first arrival time (ϵ_τ) has two contributing factors: i) due to the fact that the retrieval assumes the surface locally to be a plane (ϵ_r) ; ii) due to contribution from the instrument (ϵ_i) to the error in τ.

Sea ice freeboard is calculated by subtracting an ice elevation from some local average of the ocean elevation:

$$h_{fi}(x,t) = h_{obs} - \Delta h_{obs}(x,t) - \sum_j y_j(x,t)(h_{ssh}(x_j,t_j) + \Delta h_{ssh}(x_j,t_j))$$

$$h_{fi}(x,t) \equiv h_{obs}(x,t) - \tilde{h}_{ssh}(x,t) \qquad (3.2)$$

where $\tilde{h}_{ssh}$ is the estimate of the surface of the lead. If the lead is not present, Δh_{obs} and Δh_{ssh} are corrections that account for the tides and ocean topography at the location and time of the measurements of the ice or lead. The elevation of water (SSH) is a sum of contributions from a number of physical processes:

$$hssh\ (x, t) = hg(x) + ha(x, t) + hT(x, t) + hd(x, t) \qquad (3.3)$$

where hg is associated with geoid undulations, ha represents the atmospheric pressure loading, hT summarizes tidal contributions, and hd accounts for the ocean dynamic topography associated with geostrophic surface currents and other surface currents caused, e.g., by eddies. All these terms vary in time and

space and contribute to the uncertainty of the derived sea ice thickness (SIT) when the sea ice, water and snow height are measured relatively to the level of a reference ellipsoid. The sea ice freeboard, hfi, can be measured also as a difference between the sea ice surface or ice-snow interface.

Considering above the error (ϵ_{fi}) of the sea ice freeboard is:

$$\epsilon_{fi}(x,t) = \frac{c\left(\epsilon_{\tau_{fi}}(x,t) - \tilde{\epsilon}_{\tau_{ssh}}(x,t)\right)}{2} + \frac{\tau\left(\epsilon_c(x,t) - \tilde{\epsilon}_c(x,t)\right)}{2} + \epsilon_z(x,t) - \tilde{\epsilon}_z(x,t) + \epsilon_l(x,t) - \tilde{\epsilon}_l(x,t) \quad (3.4)$$

where ϵ_r (retrieval error), ϵ_c (propagation error), ϵ_l (ocean tide and topography model error), ϵ_i (instrument error), ϵ_z (satellite position error) will be discussed in the following sectiopns. The retrieval error (ϵ_r) depends on surface roughness and penetration.

3.1.1 Surface roughness

The statistics of the surface roughness of sea ice may not be stationary within the area illuminated by the altimeter (~ 1 km^2). If there are many corrugations within this area then the retuned echo will be sensitive to their average properties, however if the corrugation is large, or if it has a particular orientation, then the effect on the echo may be complicated and the elevation may be biased as a result. Handricks et al (2010) demonstrated that laser airborne and RA on board of satellite can be statistically biased by presence of small patches of open water or ice deformation zone.

3.1.2 Penetration error

It is generally assumed that the dominating scattering surface for the radar is from the snow/ice interface. Some observations demonstrate variations in the radar penetration depth over Arctic snow covered sea ice.

The penetration depth of radar signal depends on the snow properties. If sea ice is covered by dry, cold snow, Beaven et al. [1995] found from laboratory experiments that a Ku-band radar signal at normal incidence reflects at the snow-ice interface. In case of wet snow the radar signal does not penetrate into the snow layer, but reflects from the snow surface [Hallikainen, 1992]. Internal ice layers and ice lenses in the snow layer, snow grain size and the presence of frost flowers affect the penetration depth.

Airborne radar altimeter and in situ field measurements, collected during the CryoSat Validation Experiment (CryoVEx) on May 2006 and 2008 field campaigns have also been used to investigate the dominant scattering surface over Arctic

sea ice. Giles et al. [2007] found radar penetration to agree well with expected snow depths in Fram Strait. Results of measurements carried out north of Greenland by Willatt et al. [2011] show that in 2006 only 25% of the dominant radar return originated from closer to the snow-ice interface than to the snow surface under close to freezing temperatures while in 2008 this number increased to 80% during colder conditions (T_{2006}=-4□C and T_{2008}=-8□C). Hendricks et al. [2010] finds no penetration of the ASIRAS radar into the snow layer covering the sea ice in the Lincoln Sea (outside Alert) for neither the 2006 nor the 2008 data set. Further they find a small penetration of the radar signal of the sea ice in the Greenland Sea (Fram Strait), but with obtained depths less than the expected snow depths. Both studies by Willatt et al. [2011] and Hendricks et al. [2010] are based on data collected in late spring when the snow might not be dry and cold anymore. Ricker et al. [2012] found reflection somewhere between the snow surface and the snow-ice interface based on ESA CryoVEx 2011 data, which were collected earlier in the season (mid-April) during cold dry conditions. A similar result was found by Willatt et al. [2010] for cold Antarctic snow on sea ice. The results from these investigations suggest penetration depth dependence on temperature because in 2006, when the snow temperatures were close to freezing, the dominant scattering surface in 25% of the radar returns appeared closer to the snow/ice interface than the air/snow interface. However, in 2008, when temperatures were lower, the dominant scattering surface appeared closer to the snow/ice interface than the air/snow interface in 80% of the returns. It is important to note that the CryoSat-2 and RA estimates of sea ice thickness are only made during winter (October-March) when cold conditions may be expected. Connor et al, (2009) compare airborne laser altimetry (ATM) elevations and elevations from the Envisat radar altimeter (RA-2) over sea ice and show that the radar elevation are lower than the laser elevation. They find a mean difference in elevation of 0.36 m over floe (flat unbroken surface), which is consistent with the snow depth climatology from Warren et al (1999) and difference of 0.31cm over leads. Further CryoVEx experiments have been conducted to investigate the radar penetration into the snow layer (e.g. CryoVEx 2011). The comparison of ASIRAS and ALS data in Fram Strait from the ESA's CryoSat Validation Experiment (CryoVEx) show that the radar scattering interface depends not only on the temperature at the time of observations but also on presence of refrozen areas due to rise of the temperature in the past or due to small ice freeboard, close to the sea –water interface and presence of thick snow cover [Cicek et al 2013] or presence of open water. Hendricks et al (2010) demonstrated that airborne laser and space borne radar can be statistically biased due to presence of small patches of open water, due to impact of surface roughness or due to uncertainties in the measured freeboard from laser altimeter but not due to penetration of RA echo in the snow.

Simulations conducted by [R30] suggest that a proportion (~7%) of the altimeter radar pulse is reflected from the air-snow interface even for dry snow. This "early return" distorts the returning pulse and reduces the half power time

which results in an "effective scattering surface" somewhat above the snow-ice boundary. The extent to which this occurs, assuming that the reflectivity of the snow and ice are constant, is dependent on several parameters, the most important of which are the snow and ice surface roughness, snow thickness and density. Experimental and theoretical studies demonstrate that the ice density depends on effective scattering interface which is: i) on ice interface if it is not a snow depth; ii) on effective snow-ice interface which depends on ice freeboard, snow depth and density

3.1.3 The difference in the shape of the echo from the ice and the leads

The retrieving of the first arriving time, τ , from an echo involves fitting of radar data to a model, which describes the echo shape. The shape of radar altimeter echoes varies depending on the surface. Over the consolidated ice pack, and open-ocean, diffuse echoes are observed, however over leads the radar echoes are specular. Therefore different models are used to retrieve τ over the ice and over the leads, which results in a bias between the elevations from the ice floes and from the leads.

3.1.4 The propagation error and tidal error

3.1.4. The propagation error () and tidal error ()

The importance of these errors depends on how the difference between the ice elevation and the ocean elevation is performed. When the ice freeboard is calculated as a difference from a mean sea surface and mean ocean observations, then ϵ_c and ϵ_l is estimated by:

$$\epsilon_c(x,t) - \tilde{\epsilon}_c(x,t) \sim \epsilon_c(x,t) \quad \epsilon_l(x,t) - \tilde{\epsilon}_l(x,t) \sim \epsilon_l(x,t) \tag{3.5}$$

However, if there are enough elevation estimates from leads to extrapolate the ocean surface along the satellite track, forming an 'instantaneous' mean sea surface then

$$\epsilon_c(x,t) - \tilde{\epsilon}_c(x,t) \sim 0 \quad \epsilon_l(x,t) - \tilde{\epsilon}_l(x,t) \sim \tilde{\epsilon}_l \tag{3.6}$$

The propagation, tidal and dynamic topography errors have length scales larger than typical ice floes and therefore they cancel. The instrument errors ($\tilde{\epsilon}_l$) contain short scale geoid errors, which may lead to increased estimate of the sea surface height.

3.1.5 The speckle error

All radar echoes exhibit a form of signal distortion know as 'speckle'. As the speckle decorrelates between consecutive echoes summing over *n* echoes

reduces the noise due to speckle by $\sqrt{n}$. Therefore, for gridded ice thickness products, the errors depend on the number of observations in a particular grid cell. This quantity will vary spatially due to the convergence of the ground track at the latitudinal limit and also seasonally as the fraction of leads and ice floes varies.

3.1.6 Satellite position error

As with the propagation and tidal errors we expect that the orbit errors will cancel in the freeboard calculation. Therefore $\epsilon_z(x,t) - \tilde{\epsilon}_z(x,t) \sim 0$.

3.1.7 Sampling error (error of omission)

The radar may not sample the smallest floes and if the statistics of the sampled ice are different to the total ice cover then this will result in an error in the spatially averaged ice thickness. [*Wingham et al.*, 2001] suggest that this error could be investigated using airborne thickness measurements (laser altimetry or EM techniques) combined with imagery and by combining satellite retrievals of sea ice thickness with imagery.

Please see [*Wingham et al.*, 2001] for a description of the co-variance of the error in satellite derived sea ice thickness estimates.

The re-tracking algorithms and the collocated geophysical corrections for RA-2 altimeter and MWR data products are described in ENVISAT RA2 /MWR products manual [R24].

3.2 Errors associated with the conversion of the freeboard derived from CryoSat-2 to SIT

The main sources of errors associated with conversion of freeboard to SIT are related with: i) impact of water, ice and snow ice densities; ii) impact of snow depth. The impact of ice, snow, water density and snow depth on retrieved SIT and SID, using ULS, LA and RA is discussed in the next section.

3.2.1 Impact of Sea Ice, snow and water densities on retrieved SIT from CryoSat-2

Constant ρ_w , ρ_i , ρ_s have been used to retrieve the SIT from Cryodat-2, but the experimental observations show that ice, water and snow densities vary with time, location season and ice freeboard, which may introduce error in the retrieved SIT when constant values are considered. Experimental results, confirming variations of ice, snow and ice densities and their dependence on ice freeboard will be discussed in this section.

Sea water density, ρ_w , depends on salinity, S, temperature, T, and pressure: $\rho_\omega = \rho_\omega$ (S, T, p) (kg/m^3) and ranges from about 1022 kg/m^3 at the sea surface to 1050 kg/m^3 at the bottom of the ocean, mainly due to compression. Water density of ρ_w =1030kg/m^3 has been used to calculate SIT from the freeboard

derived from RA on board ERS, Envisat (using Algorithm A1] and by CryoSat2, (A2 Algorithm [R15]). Water density ρ_w =1025+0.5kg/m^3 has been used [Alexandrov et al, 2010] to calculate mean MYI sea ice density. The density of sea water across the Beaufort Shelf and slope off Alaska varies between 1023.2 kg/m^3 in October to 1024.2 kg/m^3 in April and a mean value of ρ_w =1024kg/m^3 has been used for SIT retrieval from ICESat [Kwok and Cunningham, 2008, R72].

Snow depth and density from WC [R12] are collocated with the same spatial and temporal resolution as RA data, where rs (kg/m3) is in the range 260-330kg/m3 for winter months, with mean, rs=295 kg/m3 and s(rs)= 24.5kg/m3.

The density of sea ice vary in wide range and depends on density of pure ice, the fractional volume of air pockets and the amount and density of brine in the ice. The density of pure ice at 0oC is 916.4kg m-3 [Hobbs, 1974] and is increasing to 919.3 kg/m3 at -30oC. The density of sea ice can be greater than these values because of the effect of brine inclusions in the ice, or less because of the effect of air bubbles [R71]. The brine volume generally increases with temperature. Timco and Frederking (1996) reported that FY ice density is typically between 840 and 920 kgm−3, while MY ice density is between 720 and 910 kgm−3. For FYI density, Schwarz and Weeks [1977] found that most observed values lay in the range 910-920kg m-3 and the ice densities calculated from isostatic relationships range from 911 to 919 kg/m3 with a mean value of 913k g/m3. Vinjea and Finnekasa [1986] drilled 382 holes in level ice of different ages in Fram Strait during July-August and obtained a mean ice density of 902 kg/m3, which was estimated in summer period with impact of melting. Kovacs and Holladay[1989] found a mean ice density of 911kg/m3 for MYI (thickness range 2-6.5 m) in the Beaufort Sea. Untersteiner [1961], has found 913kg/m3 ice density and according to Wadhams, et al, [1992] , the FY ice density range is 910-920kg/m3, but it depends on temperature, free-board, snow depth, presence of melting (e.g. 840kg/m3 FYI density is reported during the melt season [Weeks and Lee, 1958]). According to Alexandrov et al, (2010) , the ice densities of MY and FY ice below the waterline are not significantly different, and both ice types have typical values between 920 and 940 kgm−3 due to the higher volume of air-filled pores in MYI compared to FYI.

The sea ice density dependence on hfi has been documented from many authors [9, 48, 51, 71, 73]. Using the equation for isostatic equilibrium, the sea ice density has been calculated from different authors as a function of hfi, hs and rs [9, 48, 71], which confirms that point (constant) ice density will lead to essential errors in retrieved SIT for different hfi , hs and rs when the equation for hydrostatic equilibrium is applied. Assuming that the ice is in isostatic equilibrium and using Equation (3.1), snow density (rs =324 +50kgm−3), snow depth (hs) (mean 0.05m), ice thickness (hi) and ice freeboard (hfi) from Sever measurements, Alexandrov et al, [2010] estimated mean ice density for FY ice ri =916.7±35.7 kgm−3 from:

$$ri = rw - (hfirw + rshs)/hi, \quad (3.7)$$

Where water density is rw =1025+0.5kg/m3. Because the ice density depends on hfi , hs and rs the FY ice density in different locations and snow depth may be different than ri =916.7kg/m3 calculated based on Sever expedition.

By inserting density values for the upper and lower ice layers, using freeboard (0.3 m) and ice thickness 2.9 m, a mean MY ice density 882±23 kg/m3 is calculated by Alexandrov et al, (2010) from:

$$ri = ril\ (1 - hfi/hi) + riuhfi/hi \quad (3.8)$$

The estimated MYI density (882 kg/m3) is less than ri = 915 kgm−3, used from Kurtz et al, [2012] to derive SIT from OIB and the ice density 925kg/m3, used from [Kwok and Cunningham, 2008] to derive SIT from ICESat, or the ri = 900 kgm−3 used to collocate SIT from RA2/Envisat and RA/ERS 1, 2, which may lead to underestimation of SIT in comparison with SIT derived from OIB, ICESat, ERS and Envisat, if a (point) fixed ice density (882kg/m3) is used for the same conditions (freeboard, snow depth, ice type and temperature).

Experimental [Wadhams et al, 1992, R71] and theoretical studies [Kovacs, 1996] confirm the dependence of ri on ice type and hfi . Ackley et al, (1976), carried out a point-by-point isostatic analysis of MY floes, which have been profiled by drilling and tested few algorithms for free-board-to-draft conversion: i) a simple point isostatic model, using an estimated mean ice density and ii) a variable, free-board dependent (FD) density model based on regression dependence of ice density (ri) on "effective" ice free-board hfie (m). Based on surface observations (drilling) of hfi and d, Ackley et al, (1976), estimated a linear relationship between ri and "effective" ice free-board hfie (m). He found that hfie depends on sea ice freeboard hfi, snow depth hs , density rs and the mean MY ice density, riMYmean:

$$hfie = hfi + (hsrs/riMYmean) \quad (3.9)$$

Based on drilling and point by point isostatic analyses of hfi the following relationship is obtained between MYI density and hfie [Wadhams, et al 1992, Ackley et al, 1976]:

$$riMY = -a1\ hfie + b \quad (3.10)$$

where a1=194, b=948, calculated for rw=1020kg/m3. By comparison with in-situ (drilling) observations , Ackley et al, (1976) concluded that the FD ice density model provides more accurate results for F to SID conversion compared with application of point (fixed) sea ice density.

3.2.2 Impact of snow depth on retrieved SIT from CryoSat2

Snow depth is an important variable to retrieve SIT from RA, using the hydrostatic equation and only the snow depth and density from WC is available for the Arctic, in all seasons and with the same spatial resolution as the Ceyosat2 averaged area. Snow depth with higher spatial resolution in limited locations or

time of the year and unknown accuracy may be available from AMSUA or OIB radar and despite these data are not suitable for SIT retrieval from Cryosat2 the basic principles of snow depth retrieval from WC, AMSUA and OIB/radar and corresponding accuracy will be discussed in the following section.

Snow depth and density from Warren climatology

The snow depth and ice density, estimated from WC have been used successfully until now for SIT retrieval from RA/ERS, Envisat and ICESat [R54, R60], using the equations of hydrostatic equilibrium.

WC providing estimates of the monthly snow depth hs (cm), given by two-dimensional quadratic fit to measured snow depth:

hs = H0 + Ax + By + CxyDx2 + Ey2, (3.11)

where H0 is the mean monthly snow depth at the North Pole, x (latitude) and y (longitude) are positive axis respectively along 0° and 90°E in degrees and the coefficients A,B,C,D,E provide information for snow depth distribution and are listed in Table 3.1. The RMS error (ε) of the fit (in cm), the slope F of the trend lines in cm yr-1, inter-annual variability (IAV) and their uncertainty (σf) are given in Table 2.1. [Warren et al., 1999].

Table 3.1. Coefficients of snow depth approximation [R12].

Month	H_0	A	B	C	D	E	ε	F	σ_F	IAV
Aug	4.64	0.3100	−0.6350	−0.0655	0.0059	−0.0005	4.6	−0.01	0.05	3.3
Sept	15.81	0.2119	−1.0292	−0.0868	−0.0177	−0.0723	7.8	−0.03	0.06	3.8
Oct	22.66	0.3594	−1.3483	−0.1063	0.0051	−0.0577	8.0	−0.08	0.06	4.0
Nov	25.57	0.1496	−1.4643	−0.1409	−0.0079	−0.0258	7.9	−0.05	0.07	4.3
Dec	26.67	−0.1876	−1.4229	−0.1413	−0.0316	−0.0029	8.2	−0.06	0.07	4.8
Jan	28.01	0.1270	−1.1833	−0.1164	−0.0051	0.0243	7.6	−0.06	0.07	4.6
Feb	30.28	0.1056	−0.5908	−0.0263	−0.0049	0.0044	7.9	−0.06	0.08	5.5
Mar	33.89	0.5486	−0.1996	0.0280	0.0216	−0.0176	9.4	−0.04	0.10	6.2
Apr	36.80	0.4046	−0.4005	0.0256	0.0024	−0.0641	9.4	−0.09	0.09	6.1
May	36.93	0.0214	−1.1795	−0.1076	−0.0244	−0.0142	10.6	−0.21	0.09	6.3
Jun	36.59	0.7021	−1.4819	−0.1195	−0.0009	−0.0603	14.1	−0.16	0.12	8.1
Jul	11.02	0.3008	−1.2591	−0.0811	−0.0043	−0.0959	9.5	0.02	0.10	6.7

The snow density in WC varies seasonally and as the seasons change from autumn to winter the snow density increases from ~250 kg m-3 in September to ~ 320 kg m-3 in May, due to the effects of the snow settling and wind, with the highest snow density during snow melt. Snow depth and density, estimated from WC have been confirmed with in-situ monthly observations [73] in different locations in the Arctic. Alexandrov et al. (2010) examine snow density from the Sever expeditions and found an average snow density on FYI of 324 ± 50 kg m-3, which is similar to rs = 310-320 kg m-3 estimated by WC. As the snow water equivalent (SWE) is a snow depth multiplied by snow density, equal snow densities over FYI and MYI will lead to similar snow depth over FYI and MYI for the same SWE

The distribution of SWE as a function of month of the year, latitude (x) and longitude (y) is calculated by Equation 2.6. and the snow density can be calculated by dividing SWE by corresponding hs (approximated by Equation 2.5) and SWE:

SWE = H0 + Ax + By + CxyDx2 + Ey2, (3.12.)

The coefficients of the SWE, RMS error and IAV are listed in Table 3.3 and are different from the coefficients in Equation 3.11.

Table 3.2. Coefficients of the fit to the snow water equivalent (SWE), the RMS error in the fit and inter-annual variability [R12].

TABLE 2. Same as Table 1 but for snow water equivalent

Month	H_0	A	B	C	D	E	ε	F	σ_F	IAV
August	1.08	0.0712	−0.1450	−0.0155	0.0014	−0.0000	1.1	−0.001	0.012	0.8
September	3.84	0.0393	−0.2107	−0.0182	−0.0053	−0.0190	2.0	−0.003	0.016	1.0
October	6.24	0.1158	−0.2803	−0.0215	0.0015	−0.0176	2.3	−0.005	0.021	1.4
November	7.54	0.0567	−0.3201	−0.0284	−0.0032	−0.0129	2.4	−0.000	0.023	1.5
December	8.00	−0.0540	−0.3650	−0.0362	−0.0112	−0.0035	2.5	−0.003	0.024	1.5
January	8.37	−0.0270	−0.3400	−0.0319	−0.0056	−0.0005	2.5	−0.005	0.024	1.6
February	9.43	0.0058	−0.1309	0.0017	−0.0021	−0.0072	2.6	−0.007	0.028	1.8
March	10.74	0.1618	0.0276	0.0213	0.0076	−0.0125	3.1	0.007	0.032	2.1
April	11.67	0.0841	−0.1328	0.0081	−0.0003	−0.0301	3.2	−0.013	0.032	2.1
May	11.80	−0.0043	−0.4284	−0.0380	−0.0071	−0.0063	3.5	−0.047	0.033	2.2
June	12.48	0.2084	−0.5739	−0.0468	−0.0023	−0.0253	4.9	−0.030	0.044	2.9
July	4.01	0.0970	−0.4930	−0.0333	−0.0026	−0.0343	3.5	0.008	0.037	2.4

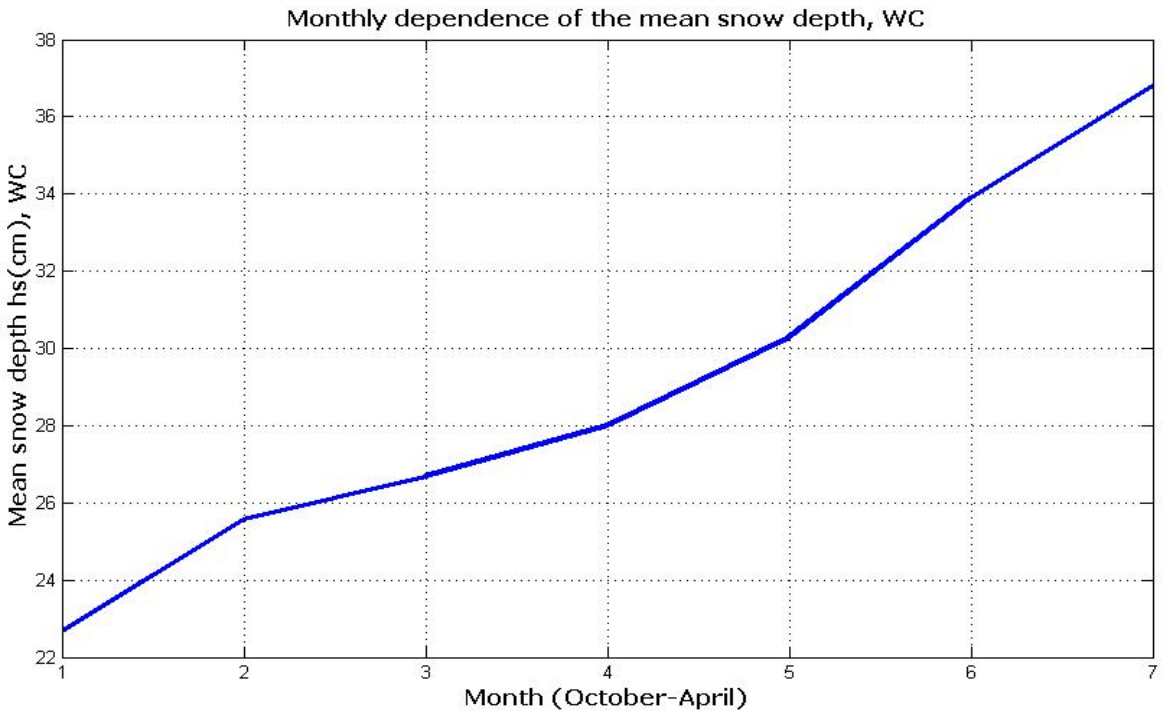

Figure 3.1. Mean Snow depth dependence, WC, October - April

The mean hs from WC for winter months (October to April) is plotted on Figure 3.1. The mean snow depth (hsmean=0.2913m) of WC for winter months is with uncertainty shs=0.049m. The difference between hs in two months (hsi+1-hsi) depends on monthly snow accumulation and location. For WC the mean monthly winter snow accumulation is only 0.02m/month with std =0.0123m, leading to SIT uncertainty of 0.0462m/month for hfi=0.3m, ri=900kg/m3, rw=1030kg/m3, rs=300kg/m3 and the uncertainty will change for different input variables (ri, rs, rw) assuming hydrostatic equilibrium (Equation 2.1).

Snow depth and density from WC have been used for CryoSat-2 algorithm validation and new algorithm development because: i) hs, rs from WC have been used until now for SIT retrieval from RA (ERS1,2,Envisat), ICESat [15,26,62] and has been validated in different studies; ii) hs, rs from WC are the only available data with the same spatial and temporal resolution as RA and CryoSat-2 averaged freeboard since 1990 and are representative for future CryoSat-2 observations; iii) The limited snow depth data from OIB radar and AMSR-E are with higher spatial and temporal resolution and unknown accuracy, requiring further algorithm improvement, which is not a task of this report. Despite the snow depth from OIB/radar and AMSR-E is not applicable for SIT retrieval from CryoSat2 in the Arctic, the algorithms and accuracy of the snow depth from OIB/radar and AMSR-E are discussed in the next section.

Snow depth from AMSR-E

The algorithm for retrieving snow depth on sea ice from AMSR-E satellite passive microwave data is based on an empirical relationship between in situ snow depths and the ratio of the normalised difference of brightness temperatures, measured by AMSRE (at 37GHz and 19GHz), assuming that the scattering increases if the snow depth increases and that the scattering efficiency is greater at 37 GHz than at 19 GHz, leading to increase of the difference between these frequencies when the snow depth increases [R11, R59]:

$$hs = a + b\,GR \quad (3.13)$$

where GR is the gradient ratio of vertically-polarized brightness temperatures (TB), compensated for sea ice concentration:

$$GR = (T37VB - T19VB)/(T37VB + T19VB) \quad (3.14)$$

The set of (a; b) coefficients are derived from brightness temperatures measured by SSM/I and snow depths, collected on Antarctic smooth FYI with a correlation coefficient of -0.77. These coefficients for AMSR-E are (2.9, -782), and they are applied in both hemispheres.

To apply this algorithm to AMSR-E measurements, AMSR-E measured TB were converted to SSM/I-equivalent TB by [Markus and Cavalieri, 2004]:

$$TSSMI19VB = TAMSRE\ 18.7VB \times 1{:}017076 - 2{:}65127; \quad (3.15)$$

$$TSSMI37VB = TAMSRE\ 36.5VB \times 1{:}016822 - 5{:}22634{:} \quad (3.16)$$

Then, TB is compensated for sea ice concentration (SIC) by:

$$TSSMIB = (TSSMIB - (1 - SIC) \times TOWB)/SIC \quad (3.17)$$

where the open water points (TOWB) are 176.6 K and 200.5 K at the frequency of 19 and 37 GHz, respectively. These tie points are from the NASA Team SSM/I algorithm. The AMSR-E snow depth algorithm accuracy is decreased essentially due to:

- Use of empirical coefficients, derived from SSMI in Antarctica;
- Missing brightness temperatures;
- Use of constant TOWB from SSM/I algorithm for AMSR-E snow depth algorithm introduce error due to instrument, atmospheric and SIC differences;
- Not applicable for SIC<0.2;
- Not applicable in presence of snow melting areas;
- Not considered impact of ice roughness, leading to decrease of the accuracy of the retrieved hs.

In addition to the above large uncertainties of the current AMSR-E snow-depth retrievals, other uncertainties were identified, including errors from snow metamorphism and from changes in atmospheric water vapour, presence of land or MYI. Snow density depends on snow depth [R73], it change with the snow type and impacts the retrieved snow depth, which is not considered because empirical constants are used for all winter months, not accounting for recent climate change impact on snow depth and precipitation. The AMSR-E snow-depth algorithm operates for a range of 170 K to 270 K TB, and allows for snow-depth retrievals up to 0.45 m [R11]. The above restrictions lead to underestimation of the snow depth, retrieved from AMSR-E, which increase as the sea ice concentration decreases [R65].

Calibration of the snow depth, derived from airborne AMSR-E simulator with the snow depth from OIB radar concluded that the current status of the accuracy of the AMSR-E snow depth algorithm is not known and it is not possible to provide accuracy of the snow depth retrieved from AMSR-E and the airborne radar because the accuracy of any of these algorithms is not known [R17]. Considering: i) already proved underestimation of the snow depth retrieved from AMSR-E [65, 67, 68]; ii) the restrictions, uncertainties of AMSR-E algorithm; iii) limited availability (only between 2002 and 2011) of AMSR-E data; iv) different spatial resolution compared with collocated RA data, it was concluded that the snow

depth, retrieved from AMSR-E data is underestimated, with unknown accuracy and cannot be used for freeboard to SIT conversion, using CryoSat-2 observations. This is confirmed also from sensitivity analyses and algorithms validation using independent ULS data.

Because the snow depth from OIB for few flights in 2009 and 2010 are also available, the accuracy of high resolution snow depth algorithm of OIB radar is discussed in the next section.

Snow depth from Operation Ice Bridge (OIB) snow radar.

OIB is developed to bridge the gap between NASA's Ice, Cloud and Land Elevation Satellite (ICESat) mission and the upcoming ICESat-2 mission [R1, http://nsidc.org/data/icebridge/index.html]. The OIB snow radar has 14.5 m × 11 m spatial resolution and after averaging of ~40 radar measurements the OIB snow depth product is with resolution 40mx11m with expected snow depth retrievals in the range 0.05 – 1.2 m [Farrell et al., 2012]. Snow depth retrievals from the OIB snow radar depend on accuracy of detection of air–snow and snow–ice interfaces within the radar signal, and determination of the spatial distance between the two interfaces. The dielectric constant depends on snow density. Very low constant snow density (264kg/m^3) has been used from Farrell, et al, 2012 to retrieve the snow depth in April 2009, considering that the mean snow density from WC for this month is ρ_s =320kg/m^3 [R12, R73] and for FYI is 324kg/m^3 [9], which impacts the accuracy of the retrieved h_s. Snow density vary from 260kg/m^3 to 430kg/m^3, which impacts the retrieved snow depth. Due to the relatively low difference between the dielectric constants for air and snow, as well as surface roughness effects, the air–snow interface is difficult to detect with OIB/radar and a threshold is set to identify the top of the snow layer within the radar return, which depends on ice snow interface and measured standard deviation, leading to snow depth dependence on sea ice freeboard (confirmed with graphics). The snow depth from the OIB radar depends on the distance between top snow air interface and bottom ice snow interface and the speed of light, which depends on snow density. Thus, use of a constant, not correct ρ_s, not accounting for snow grain and roughness, and considering the strong dependence of the algorithm on snow -ice and snow –air freeboards, may lead to inaccurate snow depth retrieval in locations with different snow density or not precise estimation of h_{fi} or h_{fs}. Considering above, an improved algorithm for snow depth retrieval from OIB/radar is required and the snow depth, derived from OIB/radar in limited locations, using the current algorithm will not be used for SIT retrieval from CryoSat-2.

Apart of the error due to contribution of sea ice, snow, water densities and snow depth the freeboard error depends on parameterisations of the radar wave propagation through the atmosphere, the Earth's gravity field (or geoid) and the ocean surface dynamic topography (determined by ocean tides, atmospheric pressure loading, currents, swell).

4 Improved CryoSat2 algorithm

The radar penetration depth depends on snow structure, grain, water content and snow density, which changes due to melt-freeze metamorphism and when the water freezes the snow density increases**.** Model simulations (Hallikainein and Ulaby, (1990)) show that the penetration depth of Ku band radar (13GHz) may decrease to about 10cm for r=0.5mm, r_s=0.24g/cm^3 and liquid water content (LWC) only 2%, which will lead to ice density contribution from an effective freeboard (h_{fe}), which depends on snow density, depth and ice freeboard.

Two CryoSat2 improved algorithms have been validated:

i) A(3) /FD Algorithm, using freeboard depended r_{iMY} over MYI (with a=214, b=948), mean ice density $r_{iFYmean}$=910kg/m^3 over FYI and information for presence of FYI, where the total ice density is:

$$r_i = fr(FY) r_{ify} + (1-fr(FY)) r_{iMY} \quad (kg/m^3) \qquad (4.1)$$

Where r_{ify} = 910kg/m^3 and the fraction fr(FY) of the FYI cover from the RA averaged area is taken from OSI –SAF [R18].

ii) FD2 Algorithm, using freeboard depended r_{iMY} over MYI, and FYI (a=-95.05, b=930.4 and $r_{iFYmean}$ =910kg/m^3 for h_{fie} <0.18m, a =-25.54, b=903.7 for h_{fie}>0.25m [R76]). It is not required a-priori information for the presence of FYI and the ice density is calculated as a function of the effective freeboard. For both algorithms, snow depth and density are calculated from WC and water density is 1024kg/m^3.

Collocated SID derived from ULS and RA freeboard, applying the improved A(FD2) Cryosat -2 algorithm are shown on Figure 4.1 and the residual of the histograms of the SID(RA,FD)-SID(ULS) are on Figure 4.1/b. One can see the decreased residual between SID(ULS) and SID(FD) and better agreement of SID(ULS) with SID(FD2).

The better performance of the FD algorithm (AFD2) over FYI and MYI is confirmed with Figure 4.1. The minimum bias and RMSE between SID, retrieved from RA and SID (ULS) and the agreement of ice density estimated for Beaufort Gyre over 4 years with that observed by Kovacs, (1996), confirms the high accuracy of the retrieved ice density and SID (RA) using A(FD2).

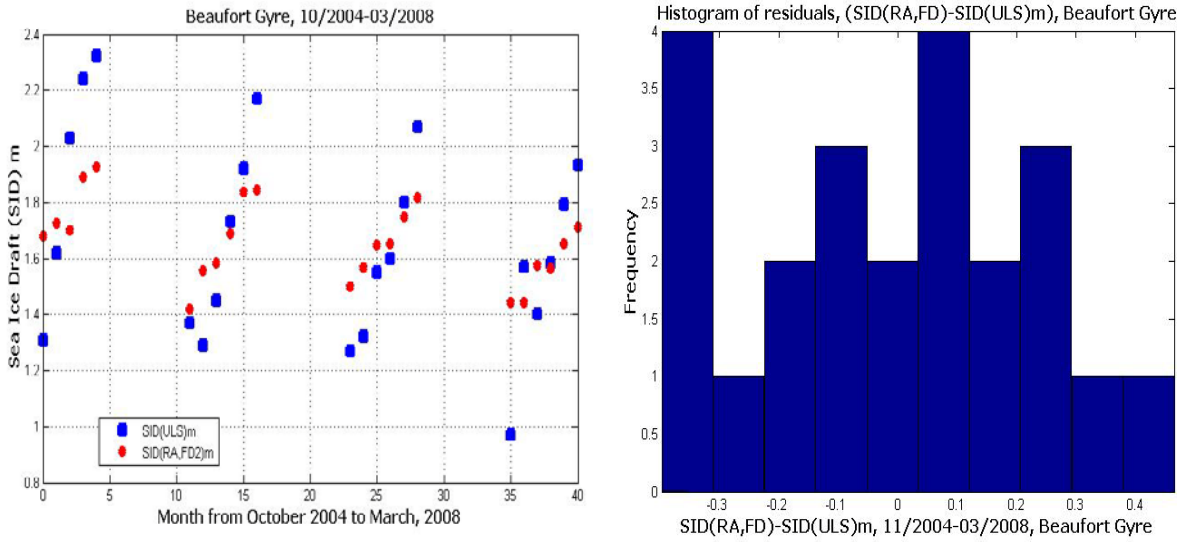

a) b) SID(RA,FD)-SID(ULS)-0.002m

Figure 4.1. Comparison of collocated SID(ULS) with SID, retrieved from RA freeboard, applying the new A(FD) and A(FD2) CryoSat algorithms: a) Collocated SID(ULS) with SID(RA, FD2), Beaufort Gyre; b)SID(RA,FD)-SID(ULS), Beaufort Gyre, 2004-2008.

5 Uncertainty of the retrieved SIT from CryoSat2

Only the uncertainties, associated with conversion of freeboard to thickness will be analysed. Assuming that the input variables in Equation 2.1 are uncorrelated, the uncertainty (s2hi) of the retrieved thickness, hi, from the freeboard, measured from CryoSat2 will depend on propagated uncertainties of the input variables [R7, R9]:

$$\sigma^2_{hi}=\sigma^2_{hfi}(dh_i/(dh_{fi})^2+\sigma^2_{hs}(dh_i/(dh_s)^2+\sigma^2_{rs}(dh_i/(d\rho_s)^2+\sigma^2_{ri}(dh_i/(\rho)^2+\sigma^2_{rw}(dh_i/(\rho_w)^2 \quad (4.1)$$

where σ^2_{hi} , σ^2_{hfi} and σ^2_{hs} are the uncertainties of the SIT, F and h_s, σ^2_{rs} , σ^2_{rw} , σ^2_{ri} are the uncertainties in the snow, water and ice densities. Uncertainty σ^2_{hfi} =0.03m [9] of freeboard, h_{fi} , retrieval from RA have been applied for all algorithms. Mean snow density, ρ_s=295 kg/m^3 and σ_{rs}= 24.5kg/m^3 is applied based on snow density from WC in winter months. The mean snow depth (0.2913m) and uncertainty, calculated for winter months from WC, have been considered, using hs from WC. Ice density for FYI ri=916.7kgm^{-3} with uncertainty ±35.7 kgm^{-3} and MYI density ρ_i = 882kg/m^3 with uncertainty +23kg/m^3[R9] are used in A2 (CryoSat-2) algorithm. Water density depends on water temperature and salinity. Water density rw =1030kg/m^3 (biased with 6 kg/m3) than the measured one in Beaufort Sea (1024kg/m3) have been used from CryoSat-2 Algorithm and the water density rw=1024kg/m3, have been used for FD (A3) and FD2 algorithm. Considering the strong dependence of sea ice density on ice type, temperature and freeboard, CryoSat-2 Algorithm is with highest ice density uncertainties (sriFY=+35.7kg/m3, sriMY=+23kg/m3) and the A3 and FD2 are with smallest uncertainties (sriMYFD= +3.45kg/m3 sriFYFD= +2.8kg/m3) estimated for up to +0.03m variations in hfi.

The percentage contribution of uncertainty (s% =s*100/mean) of input variables for A2 and updated CryoSat 2 Algorithms and the total uncertainties are given in Table 5.1.

The uncertainties s(rI) for A(FD) and A(FD) are calculated on assumption of 10% uncertainty in the freeboard for hfi=0.3cm. Improvement of the freeboard uncertainty will improve the ice density uncertainty for A(FD) and A(FD2). One can see that:

The smallest uncertainties in the retrieved SIT are observed for A(FD2), (only 2% not considering the impact of the freeboard uncertainty) and are more than 3 times less than the uncertainty of the CryoSat 2 algorithm on assumption of 10% accuracy of the freeboard;

Table 5.1 Percentage contribution of uncertainties of input variables and the total uncertainties (s%) of the calculated SIT, using the Equation for hydrostatic equilibrium

Alg.	A2/FY	A2/MY	FD	FD2/FY	FD2/MY
σ(hs i)	± 0.52%	± 0.26%	± 0.26%	± 0.26%	± 0.26%
σ□□ I)	± 3.89%	± 2.6%	± 0.38%	±0.3%	± 0.38%
σ□□ w)	± 0.58%	± 0.58%	± 0.0195%	± 0.0195%	± 0.0195%
σ□□ s)	±1.49%	±1.49%	±1.49%	±1.49%	±1.49%
σ	±6.98%	±4.93%	±2.14%	±2.07%	±2.14%

The impact of snow depth on uncertainties is negligible (0.26% for all algorithms, except for CryoSat2 over FYI (σ_{hs}=0.52%), when half snow depth over FYI is assumed;

The Sea ice freeboard accuracy and ice density are the most important factors contributing to the uncertainty.

The uncertainty of sea ice density is reduced to 0.3% when FD ice density is applied for freeboard accuracy 10%, which confirms the advantage of the FD ice density.

The uncertainties $\sigma(r_I)$ for A(FD) and A(FD2) are calculated on assumption of 10% uncertainty in the freeboard for h_{fi}=0.3cm. Improvement of the freeboard uncertainty will improve the ice density uncertainty for A(FD) and A(FD2). One can see that:

The smallest uncertainties in the retrieved SIT are observed for A(FD2), (only 2% not considering the impact of the freeboard uncertainty) and are more than 3 times less than the uncertainty of the CryoSat 2 algorithm on assumption of 10% accuracy of the freeboard;

The impact of snow depth on uncertainties is negligible (0.26% for all algorithms, except for CryoSat2 over FYI (σ_{hs}=0.52%), when half snow depth over FYI is assumed;

The Sea ice freeboard accuracy and ice density are the most important factors contributing to the uncertainty.

The uncertainty of sea ice density is reduced to 0.3% when FD ice density is applied for freeboard accuracy 10%, which confirms the advantage of the FD ice density.

6 References

R 1	Sea Ice thickness-Round Robin Data pack. User Manual	Eero Rinne, M.Makynen	2012
R2	Product Validation Plan (PVP)	www.esa-cci.org, (SICCI-PVP-05-12) 1.0	2012
R3	Sea ice thickness, freeboard, and snow depth products from Operation IceBridge airborne data.	N. T. Kurtz, S. L. Farrell, M. Studinger, N. Galin, J. Harbeck, R. Lindsay, V. Onana, B. Panzer, and J. G. Sonntag Cryosphere Discussions, 6, 4771–4827.	2012
R4	Optimization of sea ice model; using basin wide observations of Arctic sea ice thickness, extent and velocity	Miller, P. A., Laxon, S. W., Feltham, D. L., and Cresswell, D. J., J. Climate, 19, 1089–1108.	2006
R5	CryoSat: A mission to determine the fluctuations in Earth's land, marine ice field	D.J.Wingham AdvS Res37, 841–871, http://www.cpom.org/ research/djw-asr37.pdf	2006
R6	Observations of ice thickness and frazil ice in the St. Lawrence Island polynya from satellite imagery, ULS, and salinity/ temperature moorings.	R.Drucker, S.Martin, J. Geophysical Research,108, C5, 3149	2003
R7	Satellite remote sensing of sea ice thickness and kinematics a review.	R.Kwok, J. Glaciology, 56,200	2010
R8	Estimation of sea ice thickness distribution through combination of snow depth and satellite laser altimeter data.	http://ntrs.nasa.gov/archive/nasa/casi.ntrs.nasa.gov/20090038693_2009038644.pdf	2009
R9	The relation between sea ice thickness and freeboard in the arctic.	http://www.the-cryosphere-discuss.net/4/641/2010/tcd-4-641-2010-print.pdf; Alexandrov et al, Cryosphere Discussion.4, 641	2010
R10	ENVISAT RA2/MWR Product Handbook	http://envisat.esa.int/pub/ESA_DOC/ENVISAT/RA2-MWR/ra2 mwr.ProductHandbook.2_2.pdf	2010
R11	AMSR-E Algorithm. Theoretical Bases Document. Sea ice product	http://wwwghcc.msfc.nasa.gov/AMSR/atbd/seaiceatbd.pdf, .Markus, D. Cavaliery, NASA	2004

R12	Snow depth on Arctic sea ice	http://seaice.apl.washington.edu/Papers/WarrenEtal99.pdfS.Warre, I. Rigor, J. Climate,12	1999
R13	A review of sea ice density	Timco, G. W. and Frederking, Cold Reg. Sci. Technol., 24,1–6.	1996
R14	Development of seasonal pack ice in the Beaufort Sea during the winter of 1991-1992: A view from below	H. Melling and D. A. Riedel, J. GEOPHYSICAL RES., V. 101, N. C5, P 11, 975-11,991, MAY 15	1996
R15	CryoSat-2 estimates of Arctic sea ice thickness and volume	Laxon et al. GEOPHYSICAL RESEARCH LETTERS, V. 40, 1–6.	2012
R16	Comparison of Envisat radar and airborne laser altimeter measurements over Arctic sea ice	L. N. Connor, S. W. Laxon, A. L. Ridout, W. Krabill, D.McAdoo. Remote Sensing of Environment 113 563–570	2009
R17	A Comparison of Snow Depth on Sea Ice Retrievals Using Airborne Altimeters and AMSR-E Simulator(http://ntrs.nasa.gov/archive/nasa/casi.ntrs.nasa.gov/20120012935_2012011929.pdf)	Cavalieri, D.J., T.Markus, A. Ivanof, J.A. Miller, L. Brucker, M. Sturm, J. Maslanik, J. F. Heinrichs, A. J. Gasiewski, C. Leuschen, W. Krabill, J. Sonntag, IEEE	2012
R18	Ice type	http://osisaf.met.no/p/ice/#type	2012
R19	Relationship between sea ice freeboard and draft in the Arctic Basin, and implication for ice thickness monitoring	Wadhams, P., Tucker, W. B., Krabill, W. B., Swift, R. N.,Comiso, J. C., Davis, R. N.: J. Geophys. Res., 97(C12), 20325–20334	1992
R20	Airborne surveys of snow depth over Arctic sea ice	Kwok, R., B. Panzer, C. Leuschen, S. Pang, T. Markus, B. Holt, S. Gogineni. J. GEOPHYSICAL RESEARCH, VOL. 116, C11018	2011
R21	Large-scale surveys of snow depth on Arctic sea ice from Operation IceBridge,	Kurtz, N. T., and S. L. Farrell. Geophys. Res. Lett., 38.	2011
R22	The decline in arctic sea-ice thickness: Separating the spatial, annual, and inter annual variability in a quarter century of submarine data	D. A. Rothrock,1 D. B. Percival,1 and M. Wensnahan JOURNAL OF GEOPHYSICAL RESEARCH, VOL. 113, C05003, doi:10.1029/2007JC004252, 2008	2008
R23	Sea ice thickness retrieval from SMOS brightness temperatures during the Arctic freeze-up period	Kaleschke, L., et al., Geophys. Res. Lett., 39, L05501	2012

R24	Estimation of the thin ice thickness and heat flux for the Chukchi Sea Alaskan coast polynya from Special Sensor Microwave/ Imager data,1990–2001	Seelye Martin and Robert Drucker, Ronald Kwok and Benjamin Holt. J. Geophys. Res., 109, C10012, http://rkwok.jpl.nasa.gov/publications/Martin.2004.pdf	2004
R25	Retrieval of Thin Ice Thickness from Multi-frequency Polarimetric SAR Data	Kwok, R., et al., Rem. Sens. Environ., 51(3), 361-374	1995
R26	ICESat over Arctic sea ice: Estimation of snow depth and ice thickness	Kwok, R., and G. F. Cunningham, J. Geophys. Res., 113, C08010	2008
R27	The accuracy of sea-ice drafts measured from U.S. Navy submarines	Rothrock, D. A., and M. Wensnahan (2007), Journal of Atmospheric and Oceanic Technology	2007
R28	Polar Remote Sensing by CryoSat-type radar altimetry	Stenseng, L.: PhD	2011
R29	Uncertainties analyses of the retrieved sea ice draft from the Upward looking sonar, operating in the Arctic	V. Djepa, P. Wadhams, European Geophysical Union, General Assembly, Viena, 07-13/04	2013
R30	Antarctica sea ice thickness retrieval, possible limitations, uncertainties and limitations	Vera Djepa, P. Wadhams, ESA Symposium, November, 2012, Italy	2012
R31	SAR and scatterometer signatures of sea ice, in Microwave	Onstott, R. G.,Remote Sensing of Sea Ice, edited by F. D. Carsey, AGU Geophysical Monograph 68, 1st ed., chap. 5, Washington DC.	1992
R32	The physical basis for sea ice remote sensing, in Microwave Remote Sensing of Sea Ice, edited	Hallikainen, M., and D. P. Winebrenner. by F. D. Carsey, AGU Geophysical Monograph 68, 1st ed., chap. 3, Washington DC.	1992
R33	Ablation patterns of snow cover over smooth first-year sea ice in the Canadian Arctic	J. Iacozza, D. G. Barber Hydrological Processes 15, 3559–3569 (2001) DOI:10.1002/ hyp.1037	2001
R34	Arctic sea ice thickness characteristics in winter 2004 and 2007 from submarine sonar transects.	Wadhams, P., N. Hughes and J. Rodrigues. J.Geophysical Research, 116,C00E02,doi:10.1029/2011JC006982	2011
R35	Laboratory measurements of radar backscatter from bare and snow	Beaven, S. G., G. L. Lockhart, S. P. Gogineni, K. Jezek, A. R. Hosseinmostafa, A. J. Gow, D. K.	1995

	covered saline ice sheets.	Perovich, A. K. Fung, S. Tjuatja.	
R36	Rapid reduction of arctic perennial sea ice. doi:10.1029/2007GL031138.	Nghiem, S. V., I. G. Rigor, D. K. Perovich, P. Clemente-Colón, and J. W. Weatherly. Geophys. Res. Lett., 34, L19504,	2007
R37	Thickness and roughness variations of Arctic multiyear sea ice,	Ackley, S. F., W. D. Hibler III, F. Kugzruk, A. Kovacs, and W. F.Weeks,	1976
R38	A model for thermodynamic growth of sea ice in Numerical investigations of climate	Semtner A.J. Journal of Physical Oceanography, v6, May	1976
R39	Large decadal decline of the Arctic multiyear ice cover	Comiso, J. C.. J. Climate, 25, 1176-1193	2012
R40	Review of the microwave dielectric and extinction properties of sea ice and snow.	Hallikainen, M., Geoscience and Remote Sensing Symposium, IGARSS 92,International, v. 2,p. 961–965.	1992
R41	Laboratory measurements of radar backscatter from bare and snow covered saline ice sheets	Beaven, S., G. Lockhart, S. Gogineni, A. Hosseinmostafa, K. Jezek, A. Gow, D. Perovich, A. Fung, S. Tjuatja, Int. J. Rem. Sens., 16(5), 851–876	1995
R42	Monitoring ice thickness in Fram Strait.	Vinje, T., N. Nordlund, and A. Kvambekk, J. Geophys. Res., 103, 10 437–10 450.	1998
R43	Arctic-Scale Assessment of Satellite Passive Microwave Derived Snow Depth on Sea Ice using Operation IceBridge Airborne Data	Journal of Geophysical Research: Oceans,DOI 10.1002/jgrc.20228, L. Brucker, T.Marcus	2013
	Comparison of sea-ice freeboard distribution from aircraft data and CryoSat-2.	Ricker, R., S. Hendricks, V. Helm, R. Gerdes and H. Skourup: Proceedings paper, 20 years of progress in radar altimetry, 24-29 Sep., Venice, Italy, 2012.	2012
R44			
R45	Arctic-Scale Assessment of Satellite Passive Microwave Derived Snow Depth on Sea Ice using Operational IceBridge Airborne Data	Ludovic Brucker, Thorsten Markus, Journal of Geophysical Research: Oceans DOI10.1002/ jgrc.20228, 2013	2013
R46	A First Assessment of IceBridge Snow and Ice Thickness Data over Arctic Sea	Farrell, S.L., N.T. Kurtz, L. Connor, B. Elder, C. Leuschen, T. Markus, D.C. McAdoo, B. Panzer, J.	2012

	Ice	Richter-Menge, J. Sonntag	
R47	Ice Physics	Hobbs, P. V., Oxford University Press, 837 pp., New York,	1974
R48	A review of sea ice density.	Timco, G. W. and Frederking. Cold Reg. Sci. Technol., 24,1–6	1996
R49	Engineering properties of sea ice	Schwarz, J., and W. F. Weeks, . Glaciol., 19(81), 499-530	1977
R50	The ice transport through the Fram Strait,	Vinje, T. E., and O. Finnekasa, , Skr. Norsk Polarinst., 186, 1986.	1986
R51	Development of an airborne sea ice thickness measurement system and field test results, CRREL	Kovacs, A., and S. J. Holladay. Rep. 89-19, U.S. Army Cold Regions Res. and Eng. Lab., Hanover, N. H.	1989
R52	On the mass and heat budget of Arctic sea ice, Arch	Untersteiner, N., Meteorol. Geophys. Bioklimatol. Ser. A, Meteorology Geophysics, 2(2), 151-182	1961
R53	Observation on the physical properties of sea ice at Hopedale, Labrador	Weeks, W. F., and O. S. Lee, 1958. , Arctic, (3), 134-155	1958
R54	Combined airborne laser and radar altimeter measurements over the Fram Strait in May 2002.	Giles, K. A., S. W. Laxon, D. J. Wingham, D. W. Wallis, W. B. Krabill, C. J. Leuschen, D. McAdoo, S. Manizade, R. K. Raney. Remote Sens. Environ., 111, 182–194	2007
R55	Ku-band radar penetration into snow cover on arctic sea ice using airborne data	Willatt, R., S. Laxon, K. Giles, R. Cullen, C. Haas, and V. Helm, Ann.Glaciol.,52(57), 197-205	2011
R56	Effects of surface roughness on sea ice freeboard retrieval with an airborne ku-band SAR radar altimeter	Hendricks, S., L. Stenseng, V. Helm, and C. Haas, . In 30th IEEE International Geoscience and Remote Sensing Symposium, IGARSS, July 25-30, 2010.	2010
R57	A thermodynamic model for estimating sea and lake ice thickness with optical satellite data	Wang X.,Jeffrey R. Key, and Y. Liu. J. Geophysical Research. v. 115, C12035, doi:10.1029/ 2009JC005857, p.1-14.	2010

R58	BGOS ULS Data Processing Procedure	Krishfield R., A. Proshutinky. Report	2006
R59	Passive microwave algorithms for sea ice concentration - A comparison of two techniques	Comiso, J. C., D. J. Cavalieri, C. L. Parkinson, and P. Gloersen, Remote Sens.Env., 60, 357-384.	1997
R60	Arctic sea ice freeboard from IceBridge acquisitions in 2009: Estimates and comparisons with ICESat.	Kwok, R., G. Cunningham, S. S. Manizade, W. Krabil Journal of Geophys. Research 117:C02018. doi:10.1029/2011JC007654	2012
R61	The relation between Arctic sea ice surface elevation and draft: a case study using coincident AUV sonar and airborne scanning Laser	Doble, M. J., Skourup, H., Wadhams, P., Geiger, C. J. Geophys. Res., 116, C00E03,10. 1029/2011JC007076, 2011	2011
R62	Combined airborne laser and radar altimeter measurements over the Fram Strait in May 2002	Giles, K., Laxon, S., Wingham, D., Wallis, D., Krabill, W., Leusch en, C., McAdoo, D.,Manizade, S., Raney, R.: Remote Sens. Environ.,111, 182–194,	2007
R63	ASIRAS airborne radar resolves internal annual layers in the dry-snow zone of Greenland (http://epic.awi.de/ Publications/ Haw2006a.pdf),	R. L. Hawley, E. M. Morris, R. Cullen, U. Nixdorf, A. P. Shepherd, D. Wingham, Geophys. Research Letters, V. 33,L04502,doi: 10.10292005GL025147	2006
R64	CryoVEx 2011 Campaign Implementation Plan	Kjetil Lygre, M. Davidson, Duncan Wingham. Report	2010
R65	Evaluation of AMSR-E snow depth product over East Antarctic sea ice using in situ measurements and aerial photography(doi: 10.1029/	Worby, A. P. , Thorsten Markus, A. D. Steer, V. I. Lytle,R. A. Massom, J. Geophysical Res., 113, C05S94, 2007JC004181	2008
R67	ECMWF's Global Snow Analysis: Assessment and Revision Based on Satellite Observations	Matthias Drusch, D. Vasiljevic, P. Viterbo. American Meteorological Society, AMS,v43, 9/09	2004
R68	The Changing Face of Arctic Snow Cover: A Synthesis of Observed and Projected Changes	Callaghan, T. V. , M. Johansson, Daquing Yang, Ambio, 40,17-31	2011
R69	Hydrographic changes in the Canada Basin of the Arctic Ocean, 1979-1996	H. Melling, Journal of Geophysical Research, V. 103, C4, P.7637-7645, 15/4.	1998

R70	Sea ice draft in the Weddell Sea,measured by upward looking sonars.	A. Behrendt, W. Dierking, E. Fahrbach, and H. Witte, Earth Syst. Sci. Data Discuss., 5, 805-51	2012
R71	Ice in the Ocean. Amsterdam,	P. Wadhams, The Netherlands: Gordon and Breach, 368pp	2000
R72	Thinning and volume loss of the Arctic Ocean sea ice cover: 2003–2008	R. Kwok,G. F. Cunningham,M. Wensnahan, I. Rigor. H.Zwally, D. Yi, J. Geophys. Res., 114, C07005, doi:10.1029/2009JC005312	2009
R73	The snow cover of the Arctic basin	Radionov, V., Bryazgin N.,Alexandrov E., Report 1997	1997
R74	Sea ice thickness retrieval algorithms based on in situ surface elevation and thickness values for application to altimetry	Cicek B. O., Stephen Ackley, Hongjie Xie, Donghui Yi, and Jay Zwally. J. Geophysical Research, Oceans, v118, 3807-3822.	2013
	AWI CryoSat-2 Sea ice thickness Data product.	Hendricks S., R. Ricker, V. Helm Alfred Wegener Institute for Polar and Marine Research	2013
R75			
R76	Uncertainty analysis of the retrieved sea ice draft from upward looking sonar and its application for validation of the sea ice thickness derived from laser and radar altimeters	V.Djepa, P.Wadhams, under review	2013

END OF DOCUMENT